Solute Effects on β-Sn Grain Boundary Energy and Shear Stress

Michael S. Sellers[1], Andrew J. Schultz[1], David A. Kofke[1], and Cemal Basaran[2]

[1] *Dept. of Chemical and Biological Engineering, Univ. at Buffalo, State Univ. of New York, Buffalo, NY 14260.*

[2] *Electronics Packaging Laboratory, Dept. of Civil, Structural and Environmental Engineering, Univ. at Buffalo, State Univ. at New York, Buffalo, NY 14260.*

(accepted 12 October 2010; published online 15 February 2011)

The excess enthalpy and shear strain behavior of the β-Sn (101) grain boundary containing various amounts of Ag and Cu solute atoms was investigated using molecular simulation. An increase in either type of solute at the interface lowers the excess enthalpy of the grain boundary. The enthalpies of segregation for both solute types are computed as the slope of excess enthalpy of the grain boundary per area versus interfacial solute concentration per area. For Ag, ΔH^{SEG} = 0.64(9) eV/atom, and for Cu, ΔH^{SEG} = 0.45(8) eV/atom, indicating a preference for grain boundary segregation. These results agree with other simulation work that attributes a larger decrease in grain boundary energy to a solute with a larger atomic radius. A (301) special boundary of β-Sn was also investigated and found ΔH^{SEG} = 0.12(9) eV/atom for Ag and ΔH^{SEG} = 0.06(9) eV/atom for Cu. Statistically, this shows the possibility for excess enthalpy increase when Cu is present at the (301) boundary. Under constant shear strain, addition of solute lowers the yield stress of the boundary. For larger strain, yield stress levels are maintained when compared with the pure case. This indicates that the solute addition hinders sliding at the (101) interface. An interesting structural transition that occurs in the pure (101) boundary at high temperature was also explored.

Outline

Introduction

As the main component in lead-free solder joints, the behavior of Sn under various temperature and stress conditions plays a major role in how these joints exhibit damage caused by electrical currents and temperature gradients. The structure of Sn, commonly microcrystalline or polycrystalline β-Sn in solder joints, allows for a range of macroscale material strength and mass diffusion regimes (Telang 2002[32], 2004[33]; Singh and Ohring 1984[29]), resulting from both the frequency and types of boundaries created by the β-Sn grains. Among others, these properties govern the evolution of damage in the joint. Understanding how a solder material will be affected by electromigration from high current density and/or thermomigration from large temperature gradients is a step toward engineering the material for application in high-power devices and nanoelectronics.

Many factors influence the size of the grains and number of grain boundaries in a joint. Current experimental work shows that solder joints exhibit varying types of microstructure, owing in part to changing solute concentration. In 2009, Seo et al. (2009a[27]) examined Sn-*x*Ag and Sn-*x*Cu solder joints and found that microstructure was significantly affected by alloy composition and cooling rate. In a later but similar work by the same writers (2009b[28]), the time evolution of microstructure is examined during high-temperature aging, and solute concentration is shown to affect grain growth. Earlier work by Telang et al. (2004[33]) confirms the findings of Seo et al. (2009a[27]). For pure Sn ingots, reflowed Sn, and solder joints with concentrations of Ag similar to that of Seo et al. (2009a[27]), they observe a similar fine microstructure of β-Sn.

Studies at an atomistic level have investigated the effect of size, cohesive energy, and concentration of solute atoms on total grain boundary energy (E_{GB}). Millett et al. (2005a[17]) showed that Lennard-Jones solute atoms of various sizes are more effective at lowering E_{GB} than atoms of various cohesive energies. In fact, atoms with larger cohesive energies increased E_{GB}. Millett et al. (2005b[18]) also demonstrates the possibility of solute stabilization of grain growth in nanocrystals. For a nanocrystalline system of Lennard-Jones (LJ) atoms, at concentrations of solute atoms greater than 2%, all grain growth is halted during molecular dynamics (MD) simulations of the system. Furthermore, after computing the excess energy of the grain boundaries (difference from the bulk structure with solute), at these concentrations, the nanocrystalline system exhibits a lower energy than the bulk single-crystal counterpart.

The recent experimental studies on Ag and Cu solute effects on β-Sn microstructure, in addition to the solid base of theory and simulation work, present an opportunity to use molecular simulation to directly model a realistic system, with the goal of quantifying and explaining solute effects at an atomistic level. In this work, MD simulation is used to examine the effect of low-to-moderate concentrations of Ag and Cu solute atoms on the grain boundary energy of β-Sn. The (101) symmetric tilt boundary of β-Sn is simulated with varying amounts of solute, and using the modified embedded-atom method, values for the segregation enthalpy of Ag and Cu are obtained, as well as respective critical excess solute amounts. This particular boundary was investigated in a previous work by the writers (Sellers et al. 2010[26]) and shown to exhibit diffusivity close to experimental values. The writers also investigated the behavior of the solute stabilized boundaries under shear stress as a function of solute amount and compared these to simulation work investigating grain boundary slipping. Finally, some conclusions that explain some of the behavior exhibited by the solder joints in experimental work are provided.

This paper continues with a brief review of the thermodynamics of solute stabilization and stress calculation in atomistic simulation in the “Methodology” section. Next, the details of the simulation setup and data collection are explained in “Simulation Details.” The results of grain boundary energy calculations and shear stress simulations are then presented in “Results and Discussion,” and the paper ends with “Conclusions.”

Methodology

In this section, background on the theory of solute segregation at interfaces and in nanocrystalline materials is presented. The specific relations between solute concentration and grain boundary energy employed in this work are also outlined. For this study of the boundary’s behavior under shear, calculation of atomic stress and shear rates are explained.

Free Energy and Excess Enthalpy of Boundaries with Solute

When a solute atom segregates to an interface, the Gibbs adsorption equation (Gibbs 1928[10]) describes the relationship between the change of free energy of the interface (γ), the concentration of solute at the interface (Γ_A), and the chemical potential of the solute (μ_A), shown in Eq. (1). This shows that the free energy, for a positive excess amount of solute and increasing chemical potential, will be reduced

$$d\gamma = -\Gamma_A d\mu_A \qquad (1)$$

At equilibrium, the concentrations of solute in the bulk grain and at a grain boundary interface is well represented by the Langmiur-McLean adsorption isotherm (McLean 1957[16]). Eq. (2) gives the relationship between the amount of solute in the grain boundary $N_{A,\mathrm{GB}}$, the number of total atomic sites in the boundary N^{GB}, the amount of solute in the bulk matrix $N_{A,\mathrm{M}}$, and the number of atomic sites in the bulk matrix N^{M}, based on McLean’s model

$$\frac{N_A^{\mathrm{GB}}}{N^{\mathrm{GB}}-N_A^{\mathrm{GB}}} = \frac{N_A^{\mathrm{M}}}{N^{\mathrm{M}}}\exp\left(\frac{\Delta H_{A,\mathrm{M}}^{\mathrm{SOL}}-\Delta H_{A,\mathrm{GB}}^{\mathrm{SOL}}}{RT}\right) \qquad (2)$$

where $\Delta H_{A,\mathrm{M,SOL}}$ = enthalpy of solution for the solute in the bulk matrix; and $\Delta H_{A,\mathrm{GB,SOL}}$ = enthalpy of solution for the solute in the grain boundary. Weissmuller (1994[34]) extends these models to write the total free energy of a grain boundary or polycrystalline structure as

$$\gamma = \gamma_0 - \Gamma_A\left(RT\ln x_L + \Delta H_A^{\mathrm{SEG}}\right) \qquad (3)$$

In Eq. (3), the energy is now the difference between the free energy of the pure grain boundary or polycrystal (γ_0, and $\Gamma_A = 0$), and the effect of the solute on boundary configurational entropy and enthalpy terms. x_L is the solute fraction in the lattice and $\Delta H_{A,SEG} = \Delta H_{A,M,SOL} - \Delta H_{A,GB,SOL}$, the enthalpy of segregation. Neglecting entropic effects and at a constant pressure, similar to Millett et al. (2005a[17], b[18], 2007[20]), Eq. (3) can be used to calculate the decrease in potential energy of the system, upon the addition of solute at the interface. Eq. (3) is simplified below and the notation is made consistent for use in later sections of this work

$$H_{GB+S}^{EX} = H_{GB,0}^{EX} - \Gamma^{EX}(\Delta H_A^{SEG}) \qquad (4)$$

Shown in Eq. (5) and used in several works (Suzuki et al. 2005[31]; Ciccotti et al. 1983[5]) is the excess grain boundary potential energy (or enthalpy, in this work's constant pressure simulations) for a pure grain boundary, $H_{EX,GB}$. Following Eq. (5) and Fig. 1, H_{GB} is the potential energy of the grain boundary structure, H_{SLAB} is the energy of the tilted slab structure, and the quantity $N_{GB,ATOMS} \times H_{BULK,ATOM}$ is the energy of a periodic bulk structure with the same number of atoms as the slab or grain boundary. Finally, $H_{EX,GB}$ is scaled by the interface area A

$$H_{GB}^{EX} = \frac{H_{GB} - (H_{SLAB} - N_{SLAB,ATOMS} \cdot H_{BULK,ATOM}) - (N_{GB,ATOMS} \cdot H_{BULK,ATOM})}{A} \qquad (5)$$

Fig 1.

Three systems considered in excess potential-energy calculations of a grain boundary; solid lines are Miller planes and dashed lines are fixed free surfaces

View first occurrence of Fig. 1 in article.

Note that Eq. (5) can be simplified, but is left in expanded form for clarity. Starting with the potential energy of the grain boundary system, the energy increase attributed to the upper and lower free surfaces (second term of the numerator) is removed and then the remaining energy is compared to that of a fully periodic structure of the same number of atoms (third term).

For the excess energy of a grain boundary containing solute $H_{EX,GB+S}$, the calculation is slightly different. Now, the energy difference is between a grain boundary containing a given amount of solute, and a periodic bulk structure containing the same amount of solute. Since it is difficult to follow the above procedure with solute atoms included, a few additional steps are outlined to compute $H_{EX,GB+S}$. First, the energy of only the solute atoms in the bulk structure is obtained by subtracting the energy of a pure periodic bulk structure from a periodic bulk containing solute atoms. The energy of these solute atoms from the grain boundary with solute structure is then subtracted. From here, Eq. (5), where H_{GB} is now H_{GB+S}, is used to find $H_{EX,GB+S}$.

Shear Stress Calculation

Atomic level stress in these simulations is measured using the relationship for local virial stress for a given volume, which is a combination of the ideal gas and force tensors, Eq. (6)

$$\sigma_{\alpha,\beta} = -\frac{1}{V}\left[\sum_i r_i^\alpha F_i^\beta + \sum_i m v^\alpha v^\beta\right] \qquad (6)$$

where F_i = force on an atom i by its neighbors in the β direction, multiplied by the components of the position of i in the α direction of its neighbors. The second term represents the ideal gas contribution of the internal pressure of the system (found instantaneously by the kinetic energy), where m is the mass of atom i and v is the particular component of its velocity in directions α and β. V is the volume containing the atoms i included in the equation. Eq. (7) shows an expanded view of the symmetric stress tensor

$$\sigma_{\alpha,\beta} = \begin{pmatrix} \sigma_{xx} & \tau_{xy} & \tau_{xz} \\ & \sigma_{yy} & \tau_{yz} \\ & & \sigma_{zz} \end{pmatrix} \qquad (7)$$

For a system under shear, the off-diagonal term of the stress tensor describing the stress in the direction of the shear and normal to it is calculated. In this work, all shear is in the x-direction of the x-y plane, so the desired stress is τ_{xz}. It follows that the shear strain rate is given by Eq. (8), where v_x is the shear velocity in the x direction and z is the height of the simulation cell

$$\dot{\gamma} = \frac{v_x}{z} \qquad (8)$$

Simulation Details

In these simulations, the (101) symmetric tilt grain boundary of β-Sn, with varying amounts of Ag or Cu solute particles randomly placed in interstitial positions along the interface, is modeled. The (101) distinction indicates that two grains of β-Sn are rotated opposite to one another until they both share a common (101) Miller plane, equivalent to a 180° twist boundary (Sutton and Balluffi 1995[30]). The grain boundary with solute configurations is constructed with the Etomica Molecular Simulation API (2010[9]). Interactions between Sn and Ag, and Sn and Cu, are modeled with the modified embedded-atom method (MEAM) in the LAMMPS Molecular Simulator (LAMMPS 2010[15]; Plimpton 1995[22]; Huang et al. 1995[12]). Details of the potential and of this work's simulation setup and conditions are continued in the following section.

Interatomic Potential

The development of the MEAM potential is outlined below, and details are given in Baskes (1992[3], 1994[4]). The parameters of the interatomic potential were determined for Sn, and the Sn-Ag and Sn-Cu systems in Ravelo and Baskes (1997[24]), Dong et al. (2005[8]), and Aguilar et al. (2000[2]), respectively. In the model, the total energy E is given as a sum of atom energies E_i, as follows:

$$E = \sum_i \left[F_i\left(\frac{\bar{\rho}_i}{Z_i}\right) + \frac{1}{2}\sum_j \phi\left(r_{ij}\right)\right] \qquad (9)$$

where F = embedding function, or the energy required to embed an atom of type i into the background electron density ρ_i. This factor is normalized by Z_i, the number of nearest neighbors in the reference structure. The second term, $\phi(r_{ij})$, is the pair interaction between atom i and its neighbors, j. Sn, Ag, Cu, and the cross-potential parameters are listed in Table 1.

These parameters are determined by fitting experimental values of a material's bulk modulus, average atomic volume, cohesive energy, and equilibrium nearest-neighbor distance of a reference lattice structure. As reported in Ravelo and Baskes (1997[24]), the potential for Sn has successfully reproduced experimental values of the heat capacity for Sn's α and β phases, as well as the phase transition temperature between liquid and β-Sn, and β- and α-Sn. The alloy forms of the potential reflect input from experiment as well. Cu-Sn interactions reproduce a theoretical bulk diffusion activation energy of Cu in the c-direction of β-Sn lattice that is equivalent to experimental work, as well as a vacancy formation energy that is very close to experiment (Aguilar et al. 2000[2]). Similarly, for Ag-Sn interactions, the atomic volume, bulk modulus, and polycrystalline shear modulus for Ag_3Sn are reproduced almost exactly (Dong et al. 2005[8]). Details on MEAM's implementation in LAMMPS are available elsewhere (Huang et al. 1995[12]).

Structure Development, Equilibration, and Shearing Procedures

The (101) symmetric tilt grain boundary of β-Sn, which can be thought of as twist grain boundaries with 180° rotation, is constructed. The simulation cell is periodic in the directions parallel to the grain boundary interface, and fixes atoms at the top of grain one and at the bottom of grain two, mimicking a bulk structure and creating a "sandwich" of movable atoms (Keblinski et al. 1999[13]). Various quantities of solute are then randomly inserted into interstitial positions at the grain boundary interface. The final structure is shown in Fig. 2 as a normal and expanded view. In this type of setup it is important to equilibrate the system correctly to obtain a grain boundary interface of minimum energy, and to simulate at an average pressure of zero.

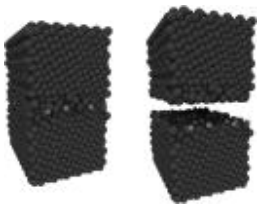

Fig 2.

Typical configuration of grain boundary with its interface loaded with solute (light gray); the left view is a simulation snapshot after equilibration and the right view is the same snapshot with the interface exposed for clarity

View first occurrence of Fig. 2 in article.

Equilibration of the grain boundary is done in three steps, followed by shear simulation. First, near 0K the two grains move independently in *x*, *y*, and *z*-directions via MD, their respective atoms all having the same average force at each time step. This step is shown in Fig. 3a.

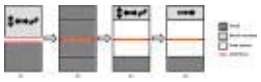

Fig 3.

(a) Grain boundary minimization (near 0K); (b) solute minimization; (c) NPT MD equilibration; (d) NVT MD shear simulation; filled arrows indicate direction of motion of the block portion; circles are solute at interface; free atoms are movable in *x*, *y*, and *z* directions; actual simulation cells are three-dimensional and periodic in *x* and *y* directions

View first occurrence of Fig. 3a in article.
View first occurrence of Fig. 3b in article.
View first occurrence of Fig. 3c in article.
View first occurrence of Fig. 3d in article.

Next, solute atoms are randomly inserted at interstitial positions in the grain boundary interface. Shown in Table 2 are the specific amounts of inserted solute and their corresponding interfacial excess density. The positions of the solute atoms are then adjusted via a conjugate gradient-energy minimization, while holding the Sn atoms fixed [Fig. 3b].

Finally, once a minimum energy configuration is found, the system is then equilibrated for 100 ps using MD with a Nose-Hoover thermostat and barostat (NPT) at the desired production run temperature and with a time step of 0.001 ps, Fig. 3c. Here, atoms in the bottom grain within twice the potential cutoff distance of the structure's bottom edge are fixed. Atoms in the top grain within twice the potential cutoff distance of the structure's top edge are given an average force in the *x*, *y*, and *z*-directions. This creates a floating boundary at the maximum z-height of the box and allows the system to reach an average pressure of zero over 100 ps. During the last 50 ps of this step, the average energies of grain boundaries with solute concentrations are collected, as shown in Table 2.

Following these steps, the floating boundary is fixed in the *y*- and *z*-directions, and moved at a constant velocity of $v_x = 5\times10^{-4}$ Å/ps in the *x* direction. Initially, the free atoms of the system are given an additional *x* velocity profile in the *z* direction to offset the sudden shock of the moving top boundary. The initial profile is linear from (v_x,*z*) points of (0.0 Å/ps, -40 Å) to (5×10^{-4} Å/ps, 40 Å). Applying Eq. (8), this is equivalent to a shear rate of $\dot{\gamma} = 6.25\times10^{6}$ s^{-1}, as all of this work's systems have a height (in *z* direction) of roughly 80 Å. During shear, systems containing various amounts of solute are simulated with constant volume (NVT) MD between nine and 15 ns [Fig. 3d] using the same time step as in Step 3. The simulation box is not deformed.

Doing work on the system in the form of shear adds energy, and for significant shear rates this can have an effect on the temperature. In this case, it is customary to either compute the temperature using a non-sheared component of the velocity (Rottler and Robbins 2003[25]) or to remove the shear effect (Horstemeyer et al. 2001[11]) by subtracting shear velocity based on an atom's location perpendicular to the shear direction (effectively removing the initial velocity profile). Although a comparably low shear rate is imposed on the system, the method of Horstemeyer et al. (2001[11]) is used to remove the shear velocity profile from the kinetic energy calculation before computing the temperature.

Results and Discussion

Molecular dynamics simulations of the (101) β-Sn grain boundary are conducted for various temperatures and solute concentrations. The average energy of each structure containing amounts of Ag and Cu, Table 2, is determined and used with the energy of the pure boundary to compute the enthalpies of segregation for Ag and Cu at different temperatures. The behavior of this boundary under a constant shear rate with 25 and 50 solute atoms is also investigated. As a complement to the excess energy calculation, measuring the boundary's response to a steady shear and observing the yield stress offers a way to qualitatively represent the structural stability of the boundary and the effect of solute atoms on boundary slip.

Excess Enthalpy Calculations

Table 2 lists the four excess solute concentrations inserted into the (101) grain boundary interface. At temperatures of 300, 350, 400, and 450K, MD simulations were used to obtain the average energies of all temperature and solute amount combinations. Following the procedure outlined in the "Methodology" section, the excess energies of the boundary with solute and the pure boundary were computed. Employing Eq. (4), $H_{EX,GB+S}$, $H_{EX,GB}$, and Γ_{EX} are known for each temperature, and ΔH^{SEG} (the enthalpy of segregation) can be solved. In Fig. 4, $H_{EX,GB+S}$, the excess energy of the grain boundary with solute, is plotted as a function of interfacial excess-solute concentration, Γ^{EX}. For data at each temperature, the weighted least-squares method was used to determine trend lines, and the slope of these lines is the solute's enthalpy of segregation. The first rows of Tables 3,4 report these values.

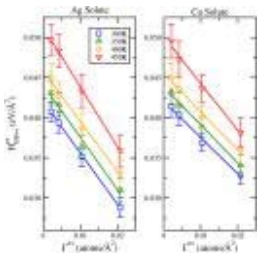

Fig 4.

Difference in the excess enthalpies of the solute-loaded grain boundary and bulk β-Sn with an equal amount of solute ($H_{EX,GB+S}$) versus excess solute concentration (Γ^{EX}); error is the standard deviation; trend lines are fitted by a weighted least-squares analysis

View first occurrence of Fig. 4 in article.

Eq. (4) also allows for a reduction in energy of the grain boundary with solute to a value equal to, or less than, that of the pure crystal. In Fig. 4, the trend lines for each temperature will intersect the *y*-axis of the plots at or near the value for the excess energy of the pure grain boundary (i.e. where $\Gamma^{ex} = 0$). In the case of a grain boundary with a given amount of solute, $H_{EX,GB+S} = 0$ represents a structure with no energy difference in comparison to the bulk structure with solute. From Eq. (4), as solute is added to the grain boundary (and corresponding bulk structure), the excess energy of the boundary will eventually be reduced to $H_{EX,GB+S} = 0$. At this point, the critical excess solute concentration is denoted as Γ_{CR}. This, along with the actual number of solute atoms for the system $N_{A,CR}$ is reported in the remaining rows of Tables 3,4 for Ag and Cu solute additions.

Segregation Enthalpies from Molecular Simulation

From the slope of the fitted lines in Fig. 2, both Ag and Cu lower the excess energy of the boundary when

compared to the bulk structure containing the same amount of solute. After computing values for ΔH^{SEG} for both solutes, it is clear that Ag lowers the energy more for an equal amount of solute and accordingly, has a larger driving force for grain boundary segregation. A larger ΔH^{SEG} corresponds to a smaller number of atoms required to meet the critical excess interface concentration, Γ_{CR}. This behavior is consistent with the trends observed by Millett et al. (2005a[17], b[18]). Millett et al. (2005a[17], b[18]) modeled a Cu Σ5 grain boundary with solute using the LJ potential. For the Cu system in reduced units, the atomic cohesive energy was ε_{Cu} = 1.0, and the atomic radius was σ_{Cu} = 1.0. By creating solute atoms of separate species, ε_{sol} and σ_{sol}, with parameters ranging from values less than to greater than ε_{Cu} and σ_{Cu}, respectively, the effect of solute cohesive energy and size on $H_{EX,GB+S}$ was evaluated. Solute atoms with $\varepsilon_{sol}<\varepsilon_{Cu}$ slightly lowered $H_{EX,GB+S}$ compared to the pure grain boundary, and $\varepsilon_{sol}>\varepsilon_{Cu}$ slightly raised $H_{EX,GB+S}$. However, any size of solute atom (σ_{sol}) lowered $H_{EX,GB+S}$, with the larger solute providing a larger decrease in energy. They attribute this effect of size to a large decrease in lattice strain energy upon segregation to the boundary. For the atoms larger than Cu, σ_{sol} = 1.6,2.0,2.4,2.8, ΔH^{SEG} = 1.12,2.74,4.01,6.03 eV, respectively.

In the writers' system, Ag has a larger covalent radius than Cu with Sn, and both solute types have a smaller radius than Sn. The Cu-Sn alloy also has a larger cohesive energy (E_c) than Sn-Sn and Ag-Sn, with Ag-Sn the smallest. From Millett et al. (2005a[17], b[18]) the larger radius of Ag and higher cohesive energy of Cu increases and decreases the tendency for boundary segregation, respectively. However, the writers' segregation enthalpies are significantly lower than those found by Millet et al. (2005a[17], b[18]) because the solute atoms differ in size. As a consequence, more Ag or Cu atoms are required to reduce $H_{EX,GB+S}$ to zero. Comparing the critical atom number ($N_{A,CR}$) to the size of the writers' system, for lower temperature Ag and all temperatures of Cu, the number of atoms in the boundary is approaching the physical limit for a single layer. These amounts will undoubtedly have solute-solute effects that are not examined here.

An interesting contrast to the previous works by Millet et al. is a study by Namilae et al. (2002[21]), where the energy of the Al (111)-Σ3 boundary energy in the presence of a substitutional atom of Mg is investigated. Namilae et al. (2002[21]) find that for this particular low-energy twin boundary, the oversized Mg atom actually increases the excess energy. The authors explain that there is unfavorable neighbor coordination at the boundary for Mg, and this energy increase is greater than the strain energy created by inserting Mg into a position in the bulk lattice.

Segregation Enthalpies from Experimental Diffusion Measurements

Two experimental works by Divinski et al. (2001[6], 2007[7]) use low solute concentrations to measure solute grain boundary diffusivity and calculate segregation enthalpies for Ni in Cu and Ag in Cu using direct radiotracer measurement. Although atomic radius played a major role in the magnitude of segregation enthalpy, there may be other causes for particular species. In a high-temperature regime, the triple product $P = s\delta D_{GB}$ is the measured value of diffusivity in the boundary, where s = solute segregation factor,δ = grain boundary width, and D_{GB} = grain boundary diffusivity. Assuming δ is constant, measuring diffusivity again in a low-temperature regime, where all diffusion takes place in the boundary and D_{GB} can therefore be measured directly, Divinski et al. (2001[6], 2007[7]) determined the temperature dependence of s. Here, s follows an Arrhenius dependence as

$s = s_0 \exp\#(-H_S/RT)$, and H_S is the segregation factor of the solute. Divinski et al. (2001[6], 2007[7]) determined the value of H_S = 0.40(4) eV for Ag in Cu and 0.176 eV for Ni in Cu, and also reported another study of Bi in Cu, where H_S = 0.552 eV. Compared to Ni, Ag and Bi have larger atomic radii, and Bi has the largest segregation enthalpy among solutes studied for Cu. It is obvious the strain introduced by the solute atoms also played a role in H_S at the experimental level. However, in the case of Bi and Ag, solute atoms with a radius larger than the solvent produced segregation enthalpies on the order of 0.4 to 0.5 eV, significantly lower than values from Millett et al. (2005a[17], b[18]). Divinski et al. (2001[6], 2007[7]) also mentioned that a cited solute study for Au, which has a significantly larger radius than Ni and is comparable to Ag, determined the Au segregation enthalpy in Cu to be less than that of Ni.

Experimental Behavior Relating to Segregation

When comparing both experimental segregation enthalpies and those computed in the writers' work with Millett et al. (2005a[17], b[18]) from separate investigations of atomic size and cohesive energy, the combined effect of the size and interaction properties must be considered for ΔH^{SEG} to be computed within a reasonable order of magnitude. It is also important to consider that other factors may influence the driving force for boundary segregation. Divinski et al. (2001[6], 2007[7]) emphasized that thermodynamics plays a role in segregation. Clearly, a thermodynamic description of the system should consider more than atomic size and cohesive energy, and does so based on theory developed by Gibbs (1928[10]) and McLean (1957[16]) included in the "Methodology" section of this work. To this point, Kirchheim (2002[14]) has shown that at certain concentrations, solute atoms can form a thermodynamic equilibrium state from a two-phase system in which a precipitated phase exists with the solvent. Seo et al. (2009b[28]) mention experimental evidence supporting this fact; as the Ag content of their joints was increased, the microstructure became finer. However, for Cu, all low-concentration joints exhibited large β-Sn grains and only slow cooling and high Cu concentration produced a fine microstructure. This microstructure contained many dendrites of an intermetallic compound (IMC), Cu_6Sn_5, which was thought to stabilize the Sn grains. The writers' work shows a lower preference for Cu to segregate into the (101) boundary when compared to Ag, most likely because of the smaller radius and higher cohesive energy. A decrease in $H_{EX,GB+S}$ also occurs with additions of both solutes, although this decrease is greater for Ag because of the factors previously mentioned. Therefore, if the preserved fine microstructure of β-Sn is a result of decreased grain growth by way of grain boundary stabilization, it is the writers' belief that Ag addition stabilizes the boundaries. For Cu at low concentrations, the solute cannot effectively stabilize the boundaries. At higher Cu concentrations, however, it is possible that a competing precipitation reaction between Cu and Sn is dominant, forming an IMC within the grain boundaries.

Telang et al. (2004[33]) also offer an explanation for the microstructure resulting from Ag or Cu addition to Sn. In their work, orientation imaging microscopy (OIM) was used to characterize the types and distributions of β-Sn grain boundaries in ingots, reflowed specimens, and solder joints, each containing different amounts of Ag and Cu. Telang et al. (2004[33]) are able to identify the types of boundaries created between grains and to show that there is a high frequency of "special" (low energy) boundaries. As Ag concentration increases, they observe a more uniform distribution of boundary types and accredit this to the boundary-segregated Ag, effectively increasing the energy of the special boundaries and making them less likely to form during cooling. Similarly,

Telang et al. (2004[33]) contend that Cu reduces the interfacial energy, increasing the likelihood of formation.

Special and Medium Energy Boundary Simulations

Contrary to Telang et al. (2004[33]), there is no evidence of solute increasing the excess enthalpy of the (101) boundary, and as previously shown, Ag will lower the excess energy of the grain boundaries in a greater capacity than Cu for the same concentration. Work by Millett et al. (2005a[17], b[18]) with low energy LJ and Cu Σ5 boundaries supports this as well. As reported previously, however, Namilae et al. (2002[21]) introduces the idea that for some boundary-solute combinations, the enthalpy of segregation can be negative (in the writers' context) and the solute will favor the bulk lattice. To test the validity of Telang et al. (2004[33]), solute loading was simulated in a (301) grain boundary, as well as two other medium-energy boundaries. The (301) boundary was identified by Telang et al. (2004[33]) to persist in β-Sn after annealing of the sample, and characterized as a low-energy boundary. Solute additions were conducted at 300K and the segregation enthalpies for Ag and Cu, shown in Table 5, were computed. Also shown are the energies of the pure boundaries. These values indicate a very weak, yet similar preference for both Ag and Cu in the (301) boundary, and the error suggests the possibility of bulk preference (a small increase in boundary energy upon segregation). For the other two medium-energy boundaries, a reasonable preference for Ag and Cu segregation is seen, when compared to experimental H_S values. Therefore, according to simulations with the MEAM potential, while the scenario that Telang et al. (2004[33]) state is statistically possible, all indications are that Ag and Cu only lower the energy of β-Sn grain boundaries. The writers believe that the effect Telang et al. (2004[33]) saw was the Ag stabilization of medium and higher energy boundaries, and consequently, the inability for the low energy boundaries to grow and consume the medium and high energy boundaries. For Cu, at low concentrations, this solute cannot stabilize higher-energy boundaries to the required degree, and therefore the solder joints with Cu exhibit β-Sn grain growth of low energy boundaries. As was shown, the effect of Ag and Cu on higher energy boundaries is much greater than the possible effect of solute on low energy boundaries. According to experimental work and the writers's simulation results, the (301) boundary is one of the lowest energy observed in β-Sn. Accordingly, this boundary provides a good lower limit by which to judge segregation effects.

(101) Grain Boundary under Shear Strain Calculations

Computing the energy change of a β-Sn grain boundary upon solute addition with MD provides some explanation as to the behavior of the material during experiment. After reflow of the solder joint, the microstructure must arrive at some thermodynamic equilibrium and the effect of solute amount on the boundary energy can be related to boundary stability. During device operation, however, the solder joint is subject to electrical current and temperature gradients, adding more driving forces to the dynamics of the microstructure, resulting in an increase of stress on the joint. The interface behavior subject to shear strain is investigated with the (101) β-Sn grain boundary containing both Ag and Cu solute amounts of 25 and 50 atoms.

This part of the study compares the yield stress of the pure grain boundary under different constant shear rates. Fig. 5 shows this shear stress versus shear strain behavior. Decreasing shear rates by an order of magnitude gives a near-linear behavior of yield stress versus shear rate on a log/log plot. The postyield behavior of the systems undergoing the two slowest shear rates, 10^6 s^{-1} and 10^7 s^{-1}, is similar—they both maintain a level of

shear stress at about 100 MPa. A “steady-state” simulation at the slowest shear rate of 10^6 s^{-1} was also conducted. The steady-state label in Fig. 5 points to a shear simulation where the strain was stopped and held at 0.0375, and the system was simulated for 2 ns. The flat line on the lowest curve indicates the system was at a steady state and maintained its stress level. The slowest shear rate pushes the limits of what is computationally feasible for these systems, with a shear strain of 0.12 requiring 144 h using four CPUs of a Quad-core 2.27-GHz Intel Xeon L5520 Nehalem processor. The increase in accuracy by reducing the shear rate twofold or threefold, following the trend in Fig. 5, is outweighed by the large increase in simulation time. Thus, the slowest shear rate (outlined in “Simulation Details”) from this figure is used in the rest of this study.

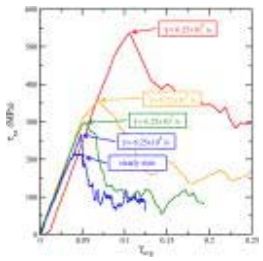

Fig 5.

Shear stress (τ_{xz}) versus average strain (γ_{avg}) for four strain rates at 300K; curve labels point to yield stress in various shear-strain rates, decreasing from top to bottom; lowest label shows the shear rate of 6.25×10^6 s^{-1} stopping at a strain of 0.0375 to simulate a steady-state condition

View first occurrence of Fig. 5 in article.

Fig. 6 shows the shear stress versus shear strain results for the pure grain boundary and two amounts of Ag solute in the interface for 300K and 450K. At 300K, the pure boundary exhibits the largest yield stress, followed by a large decrease (initial boundary slip) down to a steady shear stress of about 100 MPa. Initial loading of 25 Ag atoms causes the yield stress to drop slightly in comparison to the pure interface; yet it maintains an increased level of stress until a strain of about 0.07, where it drops to roughly 100 MPa. For 50 Ag atoms, the yield stress is larger than for the 25 atom case, and is closer to the level of the pure boundary. This interface maintains its yield stress level for a larger strain, and slips slowly to a value of 100 MPa. The curves at 300K for boundaries containing are averages of three runs with different initial configurations. Only properties are reported that are consistent between these three. At 450K, the pure boundary and boundary containing 25 Ag atoms show various points of yield stress during shear strain to 0.06. A contrasting behavior is shown when 50 atoms of Ag are present in the boundary. The stress is now distinctly higher than that of the pure boundary and 25 atom interfaces. The interface also exhibits near-elastic behavior up to its peak of about 134 MPa.

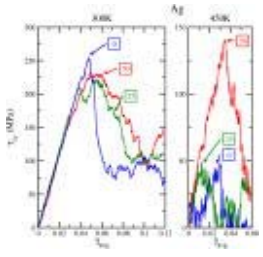

Fig 6.

Shear stress (τ_{xz}) versus average strain (γ_{avg}) for three solute amounts of Ag at 300K and 450K; number in squares are solute atom amounts; curves at 300K are the average of three independent simulation runs; note different scales for 300K and 450K

View first occurrence of Fig. 6 in article.

Many of the trends of Ag solute addition are present in the stress versus strain plots of the boundary with Cu

solute. The same shear stress versus strain behavior of the pure boundary that was shown in Fig. 6 is also shown in Fig. 7. In the case of Cu at 300K, addition of 25 atoms at the interface causes the yield stress to drop, similar to Ag. A large decrease at a strain of about 0.07 then occurs. The stress state for 50 atoms of Cu is elevated until a strain of about 0.07, where it decreases to a level comparable to the other interface concentrations. At larger strain in Fig. 7, it appears the interfaces containing solute are again increasing their level of shear stress as the strain increases. At 450K, the trends in stress versus strain are comparable to the Ag solute case. While 50 atoms of Cu also appear to increase the stress during shear strain, the level is significantly lower than the 50 Ag atom case from Fig. 6. There are also some small “shoulders” present in the increasing shear stress portion of the curve, possibly indicating various degrees of atomic rearrangement.

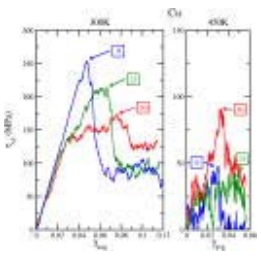

Fig 7.

Shear stress (τ_{xz}) versus average strain (γ_{avg}) for three solute amounts of Cu at 300K and 450K; number in squares are solute atom amounts; curves at 300K are the average of three independent simulation runs; note different scales for 300K and 450K

View first occurrence of Fig. 7 in article.

For both types of solute at 300K, the yield stress during boundary shear is lower after the addition of 25 solute atoms. However, a high level of stress is maintained for larger strains, compared to the pure boundary. After initial slip, shown as a rapid decrease in stress in Fig. 6,7, all the interface stress levels dropped to about 100 MPa, with the exception of 50 Cu atoms, in which the stress falls to about 125 MPa. At the higher temperature of 450K, addition of 25 atoms of solute may increase the elasticity of the boundary, if only slightly, compared to the pure case. With 50 atoms at the interface, however, the shear stress is significantly higher and the boundary now exhibits elastic behavior. In this case, Ag addition provides a larger yield stress than Cu.

For pure Sn, the experimental value for the shear modulus is given as 17.804 GPa. This is computed by Adams (1986[1]) from an average of the single-crystal elastic constants. In the simulations, the slope of the linear elastic regions of Figs. 6,7 show a modulus for the (101) grain boundary of 5.605 GPa. Discrepancies in these values are likely caused by two factors. The first is a possible weakness in the interatomic potential. Ravelo and Baskes (1997[24]) note an under-predicted elastic constant C_{44} for β-Sn by MEAM when compared to experimental values. They also find the C_{33} constant (lattice *c*-direction) is slightly smaller (softer) than the C_{11} constant (*a*-direction), when experimentally it is shown that $C_{33}>C_{11}$. However, both MEAM values are larger than experimental values. Second, in measuring the shear modulus, a value for shear in the [010] lattice direction along the (101) plane is obtained, which is compared to an average value computed from experimental elastic constants. It is therefore not surprising that the single-crystal average differs from the calculated value for a specific lattice direction.

Boundary Sliding in Solute-Segregated Boundaries from Molecular Simulation

Simulation work by Qi et al. (2007[23]) investigates the effects of applied force on the sliding of several grain

boundaries. For MD simulations of aluminum at 750K, the critical level of shear stress necessary for sliding to occur is calculated by varying the magnitude of shear force used. Qi et al. (2007[23]) show that for boundaries with higher excess energy, a lower critical stress value and an increase in grain boundary sliding is observed. Namilae et al. (2002[21]) compute static energies of Al grain boundaries and corresponding amount of slip when under shear. Similarly, Namilae et al. (2002[21]) show that for higher energy boundaries, the sliding amount is greater. Previous work by Sellers (2010[26]) quantified the energy of the (101) β-Sn grain boundary and various others using molecular simulation. The (101) boundary had the highest energy (and highest self-diffusivity) relative to the other boundaries investigated, and from comparison with other work, the pure (101) boundary will most likely exhibit the largest amount of sliding and lowest yield stress when compared with the other boundaries studied in (Sellers 2010[26]).

Investigations of sliding resistance by Millett et al. (2006[19]) find a decrease in the excess energy of the grain boundaries upon solute addition, and a corresponding resistance to sliding. Millett et al. (2006[19]) investigated the effect of both interstitial and substitutional atoms and found that for low-energy (310)-Σ5 boundaries and higher energy boundaries, interstitial atoms and oversized substitutional atoms hindered sliding. On the other hand, undersized substitutional atoms increased sliding for the higher energy boundary. From these results, Millett et al. (2006[19]) note a correlation between enthalpy of segregation of the solute species and sliding resistance. Solute that is strongly segregating will aid in sliding resistance. Results of the writers' Ag and Cu additions into the (101) boundary follow this to some extent. Initially, the yield stress is lower for the interfaces containing 25 atoms of solute compared to the pure boundary so these boundaries will begin sliding at a lower critical stress [in the context of Qi et al. (2007[23])]. After leaving the elastic regime, however, a high stress is maintained for those interfaces containing 25 and 50 solute atoms. This high stress indicates a higher resistance to sliding at larger strains in comparison to the pure boundary.

(101) Interface Structure during High-Temperature Sliding

Taking a closer look at their sliding displacement versus time plots, Qi et al. (2007[23]) discuss a change from a linear to parabolic slope as the force changes. This change is attributed to an increase in atomic disordering at the interface, where a parabolic slope is created by a large shear force perturbing the boundary region and increasing the atomic mobility. As the applied shear force increases, the mobility of the atoms at the interface increases.

The pure boundary undergoes a similar transition at 450K, as time progresses during the constant-shear velocity simulation. Initially, the interface becomes disordered over a 10–15 Å width that is perpendicular to the interface. This is followed by coexisting regions of ordered planes of atoms and mobile pocket of disordered atoms, maintained until a strain of about 0.04. At this point, there is a transition into a structure that envelops the entire interface plane. The new phase in the interface, which is five atomic layers thick, slides relative to the β-Sn lattice on planes above and below it as shear progresses.

This final structure is illustrated in Fig. 8. Planes of the new structure have formed at the grain boundary interface. The presumed lattice structure is highlighted. Figs. 8a and 8b show the side views in two different planes. Fig. 8c shows a top view of the atoms in the new structure as well as the separated planes. As is shown,

the structure is a tetragonal body-centered lattice with equal *x* and *y* lengths, and a larger *z* length than the other two. This is a deviation from β-Sn's tetragonal lattice, where the *z* length is shorter than *x* and *y*. The normal stresses of the simulation box were examined in an attempt to verify if the lattice at the interface was under compressive stress or tensile stress in a particular direction. Compressive stresses in *x*- and *y*-directions would indicate deviation from the β-Sn structure, as would tensile stress in the *z*-direction. However, stresses in *x* and *y* were opposite of each other, and the *z*-direction was under compression.

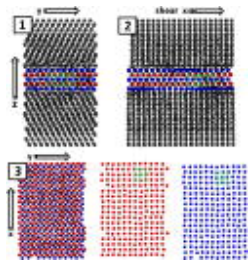

Fig 8.

Structural formation in pure GB interface at 450K under shear: (a) side view in *y*-*z* plane; (b) side view in *x*-*z* plane, shear direction indicated; (c) top view of full BCC structure and separate lattice planes

View first occurence of 8ain article.
View first occurence of 8bin article.
View first occurence of 8cin article.

The writers conclude that the many-body nature of the potential, along with the specific strain distance in the *x*-*z* direction, is assumed to aid in forming this secondary phase. After formation, this phase is maintained throughout the duration of the simulation and provides a low stress slip plane for the (101) boundary. Interfaces containing solute do not exhibit this secondary phase formation and consequently offer an increased resistance to sliding.

Conclusions

The excess enthalpy of the β-Sn (101) grain boundary containing various amounts of Ag and Cu solute atoms was investigated, as well as its behavior under shear strain. An increase in either type of solute at the interface lowered the excess enthalpy of the grain boundary. The enthalpies of segregation for both solute types are then computed as the slope of excess enthalpy of the grain boundary per area versus interfacial solute concentration per area. Under constant shear strain, addition of solute lowers the yield stress of the boundary, but for larger strain, stress levels are maintained when compared to the pure case.

Ag solute showed a greater driving force for segregation and thus lowers the excess energy of the boundary more than Cu for a given number of atoms for the (101) boundary. Research from other authors (Teland 2004[33]; Seo et al. 2009a[27], b[28]) discuss the change in microstructure for different amounts of solute in Sn-*x*Ag and Sn-*x*Cu solder joints, with Ag addition aiding in destabilizing low energy boundaries and high-concentration Cu addition forming Sn-Cu IMC, thereby pinning β-Sn grains. In regards to Ag, only a reduction in excess grain boundary enthalpy is observed, showing the beginnings of (101) interface stabilization. A short investigation of the (301) and two medium-energy boundaries found very low, but positive, segregation enthalpies for Ag and Cu in the low energy boundary and experimentally comparable segregation enthalpies for the (310) and (201) boundaries. However, considering the statistical uncertainty in the (301) results, these values indicate that an increase in that particular boundary's excess energy is possible. One experimental case was found where a Σ3

boundary's energy increased with a Mg addition. However, numerous experimental works show solute atoms stabilizing grain boundaries, both low and high energy, as indicated by the solute's positive enthalpies of segregation (in this work's context). To completely rule out the possibility of "destabilization" by Ag solute, however, more specific investigations should be carried out.

Cu and Ag solute both affected the behavior of the (101) boundary under constant shear strain. At 300K, the pure boundary exhibited the highest yield stress. Interfaces with either Ag or Cu, however, maintained a high level of stress after yield, followed by a quick decrease in stress to a value similar to that of the pure boundary. High-temperature shear brought about almost no stress response from the pure boundary, and the initially disordered interface underwent a structural transition into a tetragonal body-centered structure at long simulation time. With solute addition, however, the boundary showed less disorder and no structural transitions. Large solute concentrations produced elastic behavior from the boundary under shear, and yield stress values were about 50% and 25% of the 300K case for Ag and Cu, respectively. Overall, Ag and Cu solute addition at low- and high-temperature restricts β-Sn (101) grain-boundary sliding, evidenced by elevated values of stress at larger strains.

Acknowledgments

This research project was sponsored by the National Science Foundation under Grant Nos. CMS-0508854 and CHE-0626305, and the United States Navy Office of Naval Research, Advanced Electrical Power Systems. Computing resources were provided in part by the University at Buffalo Center for Computational Research.

Tables

Table I. Parameters for the MEAM Potential

	E_C (eV)	r_0 (A)	α	A	$\beta^{(0)}$	$\beta^{(1)}$	$\beta^{(2)}$	$\beta^{(3)}$	$t^{(1)}$	$t^{(2)}$	$t^{(3)}$	ρ_0
Sn	3.08	3.44	6.20	1.0	6.2	6.0	6.0	6.0	4.5	6.5	-0.183	1.0
Cu	3.62	2.50	5.106	1.07	3.62	2.2	6.0	2.2	3.14	2.49	2.95	1.0
Ag	2.85	2.89	5.89	1.06	4.46	2.2	6.0	2.2	5.54	2.45	1.29	1.0
Cu_3Sn	3.5	2.68	5.38									
Ag_3Sn	2.83	2.96	6.07									0.7

Table II. Ag and Cu Solute Quantities and Corresponding Excess Interfacial Density

N_s (atoms)	5	10	25	50
Γ_s (10^{-3} atoms/Å^2)	2.085	4.171	10.43	20.85

Table III. Ag Solute Calculations of Enthalpy of Segregation (ΔH^{seg}), Critical Excess Interfacial Concentration (Γ_{cr}), and Critical Number of Solute Atoms ($N_{A,cr}$)

Temperature (K)	**300**	**350**	**400**	**450**
ΔH^{seg} (eV/atom)	0.64(9)	0.65(10)	0.62(12)	0.74(14)
Γ_{cr} (10^{-3} atoms/Å^2)	66.4	68.3	74.9	66.9
$N_{A,cr}$ (atoms)	169	164	180	160

Note: Error is a weighted least-squares fit on Fig. 4—Ag slope.

Table IV. Cu Solute Calculations of Enthalpy of Segregation (ΔH^{seg}), Critical Excess Interfacial Concentration (Γ_{cr}), and Critical Number of Solute Atoms ($N_{A,cr}$)

Temperature (K)	300	350	400	450
ΔH^{seg} (eV/atom)	0.45(8)	0.47(10)	0.48(13)	0.58(14)
Γ_{cr} (10^{-3} atoms/Å^2)	92.4	93.8	96.4	85.0
$N_{A,cr}$ (atoms)	222	225	231	204

Note: Error is a weighted least-squares fit on Fig. 4—Cu slope.

Table V. Ag and Cu Solute Calculations of Enthalpy of Segregation (ΔH^{seg}) for Various Boundaries of β-Sn at 300K

Boundary	(301)	(310)	(201)	(101)
$H_{EX,GB,0}$ (10^{-2} eV/Å^2)	0.8775	2.152	2.658	4.239
Ag ΔH^{seg} (eV/atom)	0.12(9)	0.49(8)	0.44(8)	0.64(9)
Cu ΔH^{seg} (eV/atom)	0.06(9)	0.54(8)	0.37(8)	0.45(8)

Note: Error is a weighted least-squares fit of $H_{EX,GB+S}$ versus Γ^{EX}.

References (34)

1. Adams, P. J. (1986). “Thermal fatigue of solder joints in micro-electronic devices.” M.S. thesis, Drapier Lab, Massachusetts Institute of Technology, Boston. |

2. Aguilar, J. F., Ravelo, R., and Baskes, M. I. (2000). “Morphology and dynamics of 2D Sn-Cu alloys on (100) and (111) Cu surfaces.” Modell. Simul. Mater. Sci. Eng., **8**(3), 335–344. [Inspec] [ISI] |

3. Baskes, M. I. (1992). “Modified embedded-atom potentials for cubic materials and impurities.” Phys. Rev. B, **46**(5), 2727–2742. [MEDLINE] |

4. Baskes, M. I., Angelo, J. E., Bisson C. L. (1994). “Atomistic calculations of composite interfaces.” Modell. Simul. Mater. Sci. Eng., **2**(3A), 505–518. [Inspec] [ISI] |

5. Ciccotti, G., Guillope, M., and Pontikis, V. (1983). “High-angle grain-boundary premelting transition: A molecular-dynamics study.” Phys. Rev. B, **27**(9). [ISI] [ChemPort] |

6. Divinski, S., Lohmann, M., and Herzig, C. (2001). “Ag grain boundary diffusion and segregation in Cu: Measurements in the types B and C diffusion regimes.” Acta Mater., **49**, 249–261. |

7. Divinski, S., Ribbe, J., Schmitz, G., and Herzig, C. (2007). “Grain boundary diffusion and segregation of Ni in Cu.” Acta Mater., **55**, 3337–3346. |

8. Dong, H., Fan, L., Moon, K., Wong, C. P., and Baskes, M I.. (2005). “MEAM molecular dynamics study of lead free solder for electronic packaging applications.” Modell. Simul. Mater. Sci. Eng., **13**(8), 1279–1290. [Inspec] |

9. *Etomica Simulation API*. (2010). ⟨http://www.etomica.org⟩. |

10. Gibbs, J. W. (1928). *Collected works*, Vol. 1, Longmans Green and Co., New York. |

11. Horstemeyer, M. F., Baskes, M. I., and Plimpton, S. J. (2001). “Length scale and time scale effects on the plastic flow of fcc metals.” Acta Mater., **49**, 4363–4374. |

12. Huang, H., Ghoniem, N., Wong, J., and Baskes, M. I. (1995). "Molecular dynamics determination of defect energetics in beta-SiC using three representative empirical potentials." Modell. Simul. Mater. Sci. Eng., **3** (5), 615–627. |

13. Keblinski, P., Wolf, D., Phillpot, S. R., and Gleiter, H. (1999). "Structure of grain boundaries in nanocrystalline palladium by molecular dynamics simulation." Philos. Mag. A, **79**(11), 2735. [Inspec] [ISI] [ChemPort] |

14. Kirchheim, R. (2002). "Grain coarsening inhibited by solute segregation." Acta Mater., **50**, 413–419. [ISI] |

15. *LAMMPS Simulator*. (2010). ⟨http://lammps.sandia.gov⟩. |

16. McLean, D. (1957). *Grain boundaries in metals*, Clarendon Press, Oxford, UK. |

17. Millett, P. C., Selvam, R. P., and Saxena, A. (2005a). "Atomistic simulation of grain boundary energetics: Effects of dopants."Acta Mater., **53**, 3671–3678. |

18. Millett, P. C., Selvam, R. P., and Saxena, A. (2005b). "Molecular dynamics simulations of grain size stabilization in nanocrystalline materials by addition of dopants."Acta Mater., **46**(2), 297–303. |

19. Millett, P. C., Selvam, R. P., and Saxena, A. (2006). " Molecular dynamics simulations of dislocation activity in single-crystal and nanocrystalline copper doped with antimony." Mater. Sci. Eng. A, **431**, 92–99. [Inspec] |

20. Millett, P. C., Selvam, R. P., and Saxena, A. (2007). "Stabilizing nanocrystalline materials with dopants." Acta Mater., **55**, 2329–2336. |

21. Namilae, S., Chandra, N., and Neigh, T. G. (2002). "Atomistic simulation of grain boundary sliding in pure and magnesium doped aluminum bicrystals." Scr. Mater., **46**, 49–54. |

22. Plimpton, S. J. (1995). "Fast parallel algorithms for short-range molecular dynamics." J. Comput. Phys., **117**, 1–19. |

23. Qi, Y., and Krajewski, P. E. (2007). "Molecular dynamics simulations of grain boundary sliding: The effect of stress and boundary misorientation." Acta Mater., **55**, 1555–1563. |

24. Ravelo, R., and Baskes, M. I. (1997). "Equilibrium and thermodynamic properties of grey, white, and liquid tin." Phys. Rev. Lett., **79**(13), 2482–2485. [ISI] |

25. Rottler, J., and Robbins, M. (2003). "Shear yielding of amorphous glassy solids: Effect of temperature and strain rate."Phys. Rev. E, **68**, 011507. [MEDLINE] |

26. Sellers, M. S., Schultz, A. J., Basaran, C., and Kofke, D. A. (2010). "Beta-Sn grain-boundary structure and self-diffusivity via molecular dynamics simulations." Phys. Rev. B, **81**(13), 134111. |

27. Seo, S.-K., Kang, S. K., and Shih, D.-Y. (2009). "An investigation of microstructure and microhardness of Sn-Cu and Sn-Ag Solders as functions of alloy composition and cooling rate." J. Electron. Mater., **38**(2), 257–265. [Inspec] |

28. Seo, S.-K., Kang, D. K., Shih, D.-Y., and Lee, H.-M. (2009). "The evolution of microstructure and microhardness of Sn-Ag and Sn-Cu solders during high temperature aging." Microelectron. Reliab., **49**, 288–295. [Inspec] |

29. Singh, P., and Ohring, M. (1984). "Tracer study of diffusion and electromigration in thin tin films." J. App. Phys., **56**(4), 899–907. [ISI] |

30. Sutton, P. G., and Balluffi, P. G. (1995). *Interfaces in crystalline materials*, Clarendon Press, Oxford, UK. |

31. Suzuki, A., and Mishin, Y. (2005). "Atomic mechanisms of grain boundary diffusion: Low versus high temperatures." J. Mater. Sci., **40**, 3155–3161. [Inspec] |

32. Telang, A. U., Bieler, T. R., Choi, S., Subramanian, K. N., et al. (2002). “Orientation imaging studies of Sn-based electronic solder joints.” J. Mater. Res., **17**(9), 2294–2306. [ISI] |

33. Telang, A. U., Bieler, T. R., Lucas, J. P., Subramanian, K. N., Lehman, L. P., Xing, Y., Cotts, E. J., et al. (2004). “Grain-boundary character and grain growth in bulk tin and bulk lead-free solder alloys.” J. Electron. Mater., **33**(12), 1412–1423. [Inspec] |

34. Weissmuller, J. (1994). “Alloy thermodynamics in nanostructures.” J. Mater. Res., **9**(1), 4–7. [ISI] |